Heliyon 10 (2024) e35339

Contents lists available at ScienceDirect

Heliyon

journal homepage: www.cell.com/heliyon

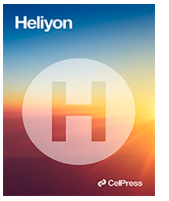

Research article

ScRNAs reveals high-frequency rTMS-induced pericyte differentiation: Potential implications for vascular regeneration and blood-brain barrier stability in stroke

Jiantao Zhang [1], Jiena Hong [1], Jiemei Chen, Fei Zhao, Qiuping Ye, Yilong Shan, Chao Li [**], Hongmei Wen [*]

Department of Rehabilitation Medicine, The Third Affiliated Hospital, Sun Yat-Sen University, Guangzhou, 510630, China

ARTICLE INFO

Keywords:
Single-cell sequencing
High-frequency repetitive transcranial magnetic stimulation
Stroke
Blood-brain barrier
Pericyte

ABSTRACT

Stroke is a major cause of adult disability worldwide, often involving disruption of the blood-brain barrier (BBB). Repairing the BBB is crucial for stroke recovery, and pericytes, essential components of the BBB, are potential intervention targets. Repetitive transcranial magnetic stimulation (rTMS) has been proposed as a treatment for functional impairments after stroke, with potential effects on BBB integrity. However, the underlying mechanisms remain unclear. In this study using a transient middle cerebral artery occlusion (tMCAO) rat model, we investigated the impact of rTMS on post-stroke BBB. Through single-cell sequencing (ScRNAs), we observed developmental relationships among pericytes, endothelial cells, and vascular smooth muscle cells, suggesting the differentiation potential of pericytes. A distinct subcluster of pericytes emerged as a potential therapeutic target for stroke. Additionally, our results revealed enhanced cellular communication among these cell types, enriching signaling pathways such as IGF, TNF, NOTCH, and ICAM. Analysis of differentially expressed genes highlighted processes related to stress, differentiation, and development. Notably, rTMS intervention upregulated Reck in vascular smooth muscle cells, implicating its role in the classical Wnt signaling pathway. Overall, our bioinformatics findings suggest that rTMS may modulate BBB permeability and promote vascular regeneration following stroke. This might happen through 20 Hz rTMS promoting pericyte differentiation into vascular smooth muscle cells, upregulating Reck, then activating the classical Wnt signaling pathway, and facilitating vascular regeneration and BBB stability.

1. Introduction

Stroke is ranked as the second most fatal and incapacitating ailment globally, with ischemic stroke (IS) constituting 75 %–80 % of all stroke subcategories [1,2]. Central to stroke progression is the disruption and subsequent restoration of the blood-brain barrier

* Corresponding author.
** Corresponding author.
E-mail addresses: zhangjt79@mail2.sysu.edu.cn (J. Zhang), hongjn5@mail2.sysu.edu.cn (J. Hong), chenjm256@mail2.sysu.edu.cn (J. Chen), zhaof65@mail2.sysu.edu.cn (F. Zhao), yeqp3@mail.sysu.edu.cn (Q. Ye), shanylong@mail.sysu.edu.cn (Y. Shan), lichao25@mail2.sysu.edu.cn (C. Li), wenhongm@mail.sysu.edu.cn (H. Wen).
[1] These authors contributed equally to this work.

https://doi.org/10.1016/j.heliyon.2024.e35339
Received 11 April 2024; Received in revised form 14 July 2024; Accepted 26 July 2024
Available online 30 July 2024

(BBB) [3]. Ischemic stroke leads to BBB breakdown due to vascular damage from ischemia-reperfusion injury, allowing blood-borne cells and molecules to infiltrate brain tissue and initiate neuroinflammatory responses and neuronal injury [3]. Pericytes, crucial for BBB integrity, reside on brain microvascular endothelial cells [4]. In response to stroke, pericytes contribute to BBB disruption through the release of inflammatory mediators and proteases under conditions of ischemia-induced inflammation and oxidative stress [5]. Conversely, they facilitate BBB repair by secreting growth factors and matrix proteins that promote the regeneration of vascular endothelial cells [6]. Thus, pericytes play a critical role in modulating BBB dynamics during ischemic stroke recovery.

The primary factor contributing to BBB disruption following a stroke is the occurrence of molecular and cellular events associated with blood flow disruption [3,7]. The BBB primarily comprises multicellular entities comprising pericytes, endothelial cells, astrocytes, and other constituents [8]. Pericytes, enveloping the endothelial cell layer, represent a pivotal element of the BBB and are also the initial cell type to react to hypoxia subsequent to stroke [4]. The distinctive location of pericytes at the blood-brain interface, their capacity to react to hypoxia, and their participation in angiogenesis render them highly suitable candidates for therapeutic intervention following a stroke [9]. Nevertheless, there remains a lack of comprehensive understanding regarding the mechanisms and interactions of pericytes and other cellular entities after a stroke event.

Presently, interventions such as tissue plasminogen activator (tPA) and thrombectomy are limited to a narrow timeframe within the initial hours following stroke onset, thus benefiting only a minority of affected individuals [10,11]. Consequently, investigating stroke mechanisms beyond the hyperacute phase and enhancing stroke prognosis through rehabilitation have emerged as paramount concerns in the field of global health. Repetitive transcranial magnetic stimulation (rTMS) is a non-invasive neuromodulation technique that has garnered extensive utilization in the management of post-stroke motor dysfunction, aphasia, and dysphagia [12]. Prior research has suggested that rTMS has the potential to decrease BBB permeability, improve vascular structure and morphology, and modulate cerebral perfusion effectively [13]. Nevertheless, the precise molecular mechanisms through which rTMS exerts neuroprotective effects across the BBB remain uncertain, thereby constraining its efficacy. Consequently, our study centered on pericytes and endothelial cells within the BBB, along with vascular smooth muscle cells, a crucial component of blood vessels. We conducted a single-cell sequencing analysis to examine the transcriptomic alterations in these three cell types in a stroke model following 20 Hz rTMS. Our objective was to elucidate the potential therapeutic effects of 20 Hz rTMS and the underlying mechanisms responsible for the recovery of neurological function. In summary, our research possesses the capacity to augment the single-cell atlas of stroke, thereby offering novel perspectives and pertinent evidence for future investigations concerning the mechanism of high-frequency rTMS and the clinical application of stroke treatment.

2. Materials and methods

2.1. Animals

Male Sprague-Dawley (SD) rats, aged seven weeks and weighing 230–250 g, were procured from Zhuhai Best Science Experimental Animals Co., Ltd. and housed at the Animal Experimental Center of South China Agricultural University under license number SYXK (Guangdong) 2022-0136. The rats were housed in a controlled environment with a 12-h light/dark cycle, consistent humidity, and temperature. They had ad libitum access to standard forage and drinking water. All procedures (Fig. 1a) involving experimental animals were approved by the Ethics Committee of South China Agricultural University (approval number: 2023d031), in accordance with ethical and regulatory standards for the use of experimental animals. The animal experiments were conducted in accordance with the ARRIVE guidelines.

2.2. tMCAO models and experimental grouping

Deep anesthesia was induced in the rats through intraperitoneal injection of pentobarbital (40 mg/kg). Transient middle cerebral artery occlusion (tMCAO) was then achieved by occluding the left middle cerebral artery for 90 min using the intraluminal suture method as previously outlined [14,15]. Throughout the surgical procedure, the rats' body temperature was maintained at 37.0 ±

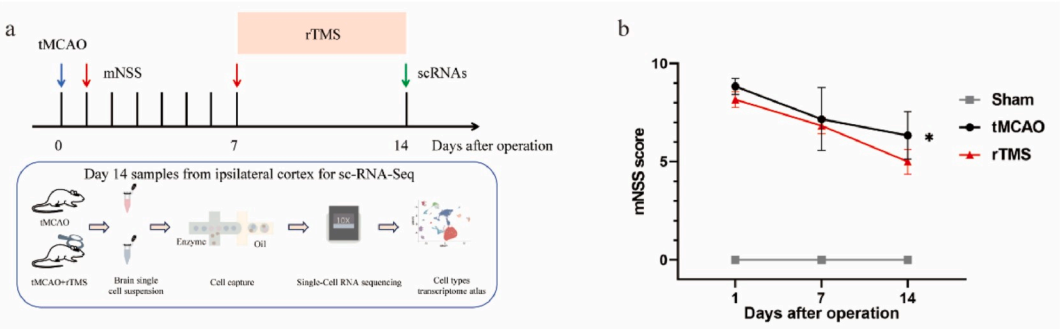

Fig. 1. Timeline and results of the mNSS score. **a.** Timeline of the experimental procedures. **b.** mNSS scores of 3 groups of rats. Results are presented as mean ± SD; N = 10; *P < 0.05, rTMS group vs. tMCAO group.

0.5 °C with a heating lamp, and appropriate postoperative care was administered. In the sham group, surgeries were performed with ligation of the external carotid artery only.

The modified neurological severity score (mNSS) was assessed for Sham, tMCAO, and rTMS groups (n = 10 per group) at 24 h, 7 days, and 14 days post-operation, with scores ranging from 0 to 18 [16]. Rats with mNSS scores of 7–12 at 24 h post-tMCAO were selected for further studies (Fig. 1b). Using a random number table, rats were allocated to either the tMCAO group (n = 2) or the tMCAO + rTMS group (n = 2) for subsequent single-cell sequencing analysis.

2.3. rTMS treatment

A customized stimulator (YRD-CCI, Wuhan, China) was utilized for administering rTMS treatment. The treatment course commenced on the 7th day post-operation and concluded on the 14th day post-operation. All procedures followed animal experimental protocols established by our research team and described in previous studies [14,17]. Specifically, a circular prototype coil (6 cm in diameter, with 3.5 T peak magnetic welds) was placed perpendicular to the cortex within the cortical surface projection region of the left frontal-parietal lobe in rats. The treatment regimen consisted of 10-s stimulation intervals followed by 50-s rest periods (repeated 10 times). The stimulation intensity was set at 33 % of the maximum stimulator output, with a frequency of 20 Hz.

2.4. Preparation of single-cell suspensions

For the preparation of single-cell suspensions, the cerebral cortex adjacent to the infarct core was promptly isolated from rats in both the tMCAO + rTMS and tMCAO groups. The Worthington Papain Dissociation System (catalog number: LK003150) was employed for this purpose. The enzymatic solution comprised 2.5 ml of EBSS, 20 U/ml of papain, and 5 U/ml of DNase I, prewarmed at 37 °C for 10 min. Subsequently, brain tissues were placed in 50 ml centrifuge tubes, rinsed with 10 ml of 1x EBSS, and then dissected into 1–2 mm^3 fragments, which were transferred to 2 ml centrifuge tubes containing 1 ml of pre-chilled 1x EBSS.

Following the addition of the enzyme mixture, the tissue underwent digestion at 37 °C with gentle agitation for 25–40 min. To halt the process, 7.5 ml of pre-chilled complete EMEM medium was introduced after digestion. The entire digestate was sieved through a 70 μm cell strainer to eliminate undigested tissue. The resultant cell suspension was centrifuged at 350 g for 5 min at 4 °C, and the supernatant was cautiously decanted. The cells were resuspended in EBSS supplemented with BSA and EDTA. Following two additional cycles of resuspension and centrifugation, the supernatant was discarded, and the cells were reconstituted in 1 ml of pre-chilled EBSS (adjustable volume), gently mixed, and filtered through a 40 μm cell strainer (pre-conditioned with EBSS) to regulate cell size. The concentration and viability of the isolated single cells were assessed using a hemocytometer and trypan blue staining.

2.5. Single-cell RNA sequencing

To begin the cellular analysis, an appropriate volume of the single-cell suspension was combined with 0.4 % Trypan Blue dye in a ratio of 9:1. Subsequently, cell counting was carried out using the Countess® II Automated Cell Counter to determine the percentage of viable cells. Ensuring that the proportion of viable cells exceeded 90 %, the cell concentration was adjusted to a desirable density of no less than 1000 cells/μL. Subsequently, the 10X Genomics 3′ transcriptome sequencing technology was utilized for conducting simultaneous transcriptome expression profiling analysis on each sample, with an average of 9039 cells. In the tMCAO + rTMS group, 9743 and 9037 cells were respectively obtained from the two samples. From the two samples of the tMCAO group, 10153 and 7225 cells were respectively acquired. PCR amplification was initiated using cDNA as the starting material. Initially, the cDNA underwent fragmentation to yield fragments approximately 200-300bp in length. Subsequently, sequencing adapters P5 and sequencing primer R1, along with other conventional library preparation steps for second-generation sequencing, were added. Eventually, PCR amplification was carried out to generate DNA libraries. The constructed libraries were subjected to high-throughput sequencing using Illumina sequencing platforms in paired-end mode. Read 1 contained 16bp barcode information and 10bp UMI information for cell quantification and expression level assessment. Read 2 harbored the cDNA fragments for alignment to the reference genome to identify the corresponding genes.

2.6. Alignment and quantification

For the generation of the raw gene expression matrix, CellRanger (version 3.0.1) was employed, and genome alignment was conducted using the STAR aligner. Rigorous quality control procedures were implemented for each sample. The processing and filtering of cells with unique molecular identifiers (UMI) were carried out using the Seurat R package (version 2.3.4) in R (version 3.6.0). Criteria included ensuring that the number of genes per cell fell within the range of the mean ± two times the standard deviation, while also restricting mitochondrial content to below 10 %.

2.7. Visualization

Within Seurat, we implemented the utilization of UMAP (Uniform Manifold Approximation and Projection) and t-SNE (t-distributed stochastic neighbor embedding), two non-linear dimensionality reduction techniques, to project complex cell data from high dimensions into a two-dimensional space. This strategic mapping enabled the clustering of cells exhibiting similar expression profiles and the segregation of cells with distinct expression patterns, thereby enhancing our ability to discern cellular discrepancies.

Subsequent to this, the application of SingleR facilitated the annotation of each cell type by comparing the expression patterns of target cells with those of reference cells, aiding in the classification of cell types based on their gene expression similarities.

2.8. Identification of DEGs

For the investigation of differentially expressed genes (DEGs) within identical cell subtypes across diverse samples or cohorts, we integrated the Model-based Analysis of Single-cell Transcriptomics (MAST) approach into the Seurat analysis platform. The evaluation of DEG significance involved employing a hurdle model to correct for multiple testing, with subsequent filtration of statistically significant genes based on criteria including $|\log_2 FC| \geq 1$, p_value_adjust≤ 0.05, and a minimum expression threshold of 10 % within the target cell population.

2.9. Gene ontology

The Gene Ontology (GO) serves as a globally recognized system for classifying gene functions, enabling the functional annotation and significant enrichment analysis of differentially expressed proteins. Comprising three distinct ontologies that delineate molecular function, cellular component, and biological process involvement of genes, GO aids in elucidating the roles of genes. In this study, differentially expressed proteins were linked to specific terms within the GO database (http://www.geneontology.org/), with the quantification of proteins associated with each term facilitating the identification of proteins with unique GO functions and their abundance. Subsequently, the enrichment of differentially expressed proteins in GO terms was assessed using a hypergeometric test against the entire background proteome. By computing p-values and applying Bonferroni correction, significantly enriched GO terms among differentially expressed proteins were identified, with a corrected p-value threshold typically set at ≤ 0.05 to denote significance.

2.10. Kyoto Encyclopedia of Genes and Genomes

Within biological organisms, the coordinated action of diverse proteins is essential for the execution of their biological functions. Pathway analysis serves to deepen our comprehension of these functions. KEGG (Kyoto Encyclopedia of Genes and Genomes) stands as a primary public repository for pathways, and pathway enrichment analysis at the level of KEGG Pathways is performed through hypergeometric testing. This analysis aims to pinpoint pathways that exhibit significant enrichment in differentially expressed proteins when compared to background proteins. Pathways meeting the criterion of a Q-value ≤ 0.05, indicative of significant enrichment in differentially expressed proteins following multiple testing corrections, are considered. Here, the Q-value denotes the FDR-corrected p-value. Through pathway enrichment analysis, crucial biochemical metabolic pathways and signaling pathways involving differentially expressed proteins can be identified.

2.11. Pseudotime analysis

Pseudotime analysis, also referred to as cell trajectory analysis, is a widely employed method for predicting the developmental paths of cell subtypes and apoptotic pathways, as well as inferring the differentiation trajectories of stem cells in the context of disease progression. In this research, we employed the Monocle software package (Version 2.10.1) to perform pseudotime analysis based on the expression profiles of pivotal genes. Through Monocle, cells along the cell trajectory are categorized into distinct differentiation states (states), with gene expression levels modeled as a smooth, nonlinear function of pseudotime values to investigate potential correlations between changes in gene expression and pseudotime values. The selection threshold was established at FDR $<$1e-5 to ensure robust results.

2.12. Cellular communication analysis

Utilizing the single-cell gene expression matrix and cell grouping data, we applied the Cellchat software to model the likelihood of intercellular communication. Subsequently, we conducted an analysis of receptor-ligand pairs by leveraging the signaling molecule interaction data integrated within CellChatDB. To enhance the robustness of our findings and minimize noise interference, we implemented the average expression algorithm in identifying significantly enriched receptor-ligand pairs across cells. By evaluating the abundance of communication probabilities associated with these receptor-ligand pairs, we delved into intercellular communication dynamics at the level of signaling pathways, investigating the regulatory implications of these key interactions. Through comparative analyses of communication disparities in receptor-ligand pairs across varied samples or groups, we scrutinized the effects of experimental interventions on the strength of intercellular communication within distinct cell subpopulations. Our objective was to unveil the underlying cellular regulatory mechanisms and communication patterns within signaling pathways.

2.13. Statistical analyses

We conducted all statistical analyses using R (version 3.6.0) and assessed statistical significance using two-tailed p values. Throughout our study, p values were computed with Bonferroni correction, and we considered $|\log_2 FC| \geq 0.25$, $P < 0.05$ as indicative of statistical significance. Within the Seurat package, we employed the rank-sum test to investigate differential gene expression across

distinct cell subpopulations.

3. Results

3.1. Identification of major brain cell types and expression of specific genes

In our investigation of the cellular composition and gene expression patterns associated with ischemic stroke (IS), we applied 10x genomics technology to analyze the mRNA transcriptomes of individual cells isolated from the rat cerebral cortex adjacent to the infarct core. Following the implementation of stringent quality control measures, we amassed a total of 36,158 cells, each exhibiting an average detection of 5110 unique molecular identifiers (UMIs). Furthermore, the UMAP plot adeptly integrated data from diverse sources, serving as a demonstration of the successful amalgamation of the acquired dataset (Fig. 2a). By considering cell types and the expression of specific marker genes, we identified 13 distinct cell clusters. These clusters included astrocyte (Slc1a3, Aqp4, Gja1), endothelial cell (Tie1, Pecam1, Icam1), microglia (Ctss, P2ry12, Cx3cr1, Tmem119), macrophage (Aif1, Mrc1, Lyz2), neuron (Snap25, Syp, Tubb3), oligodendrocyte (Mbp, Plp1, Mog), pericyte-endothelial cell (Abcc9, Kcnj8, Myl9, Rgs5, Tie1, Pecam1, Icam1), pericyte (Abcc9, Kcnj8), SMC (Myl9, Acta2, Mylk, Tagln, Sncg), perivascular fibroblast-like cell (Dcn, Bgn, Osr1, Lum, Col1a1), T cell (Cd8, Cd3), B cell (Ms4a1, Cd19), ependymal cell (Clic6, Rsph4a, Kcnj13) (Fig. 2b). In Fig. 2d, a circular plot illustrates the relative expression changes of different cell types within each group. The percentage of pericyte in the tMCAO + rTMS group (2.77 %) is slightly higher than that in the tMCAO group (2.54 %) (Fig. 2d).

3.2. Pericyte subclusters heterogeneity analysis

The breakdown of the BBB is recognized as a key characteristic observed in IS, with pericytes playing a vital role in upholding BBB integrity. To delve deeper into the transcriptional alterations within pericyte subclusters post-IS, we specifically isolated pericytes (cluster 3) from the dataset depicted in Fig. 2c and conducted subsequent clustering analysis. By re-annotating and identifying upregulated genes in pericyte subclusters, and adjusting the resolution to 0.1, we ultimately obtained 3 distinct pericyte subclusters: pericyte subcluster 0 (Rgs5, Igfbp7, Cald1), pericyte subcluster 1(Fcgr2a, P2ry12, Ccr5) and pericyte subcluster 2(Ptprb, Flt1, Cyyr1) (Fig. 3a). Utilizing a circular plot, we visually represented the cell frequencies of pericyte subgroups sourced from various sample origins. While our findings indicated an increasing trend in the cell percentage of pericyte subcluster 1 and a decreasing trend in subcluster 2 within the rTMS group compared to the tMCAO group, these observed differences did not reach statistical significance (Fig. 3b). Subsequently, we proceeded with GO and KEGG analyses focusing on the differentially expressed genes (DEGs) among these three distinct pericyte subclusters to explore their heterogeneity. For each subcluster, we identified and examined the top 15 GO terms and pathways.

Enrichment analysis of pericyte subcluster 0 revealed significant enrichment in processes related to phosphorylation metabolism, protein modification, regulation of molecular functions, response to chemical stimuli, and the mitochondrial respiratory chain (Fig. 3d). Notably, KEGG analysis primarily showed enrichment in pathways such as amoebiasis, chemical carcinogenesis - reactive oxygen species cluster, oxidative phosphorylation, diabetic cardiomyopathy, Parkinson's disease, non-alcoholic fatty liver disease, neurodegenerative pathways - multiple diseases, Huntington's disease, Alzheimer's disease, amyotrophic lateral sclerosis, thermogenesis, retrograde endocannabinoid signaling, focal adhesion, small cell lung cancer, and cancer pathways, among others(Fig. 3g).

Conversely, pericyte subcluster 1 exhibited enrichment primarily in processes related to cell activation, stress response, regulation of biological processes, immune response, cell death regulation, and intracellular components (Fig. 3e). Analysis using the KEGG database indicated enrichment in pathways such as lysosome function, antigen processing and presentation, phagosome activity, osteoclast differentiation, tuberculosis-related pathways, Chagas disease, leishmaniasis, COVID-19, apoptosis, alcoholic liver disease, pertussis, legionellosis, human cytomegalovirus infection, IL-17 signaling, and toxoplasmosis among others (Fig. 3h).

Furthermore, enrichment analysis revealed that pericyte subcluster 2 was predominantly enriched in intracellular processes and the regulation of biological processes (Fig. 3f). KEGG analysis indicated enrichment in pathways such as endocytosis, prostate cancer, human cytomegalovirus infection, Parkinson's disease, thermogenesis, cocaine addiction, oxidative phosphorylation, Huntington's

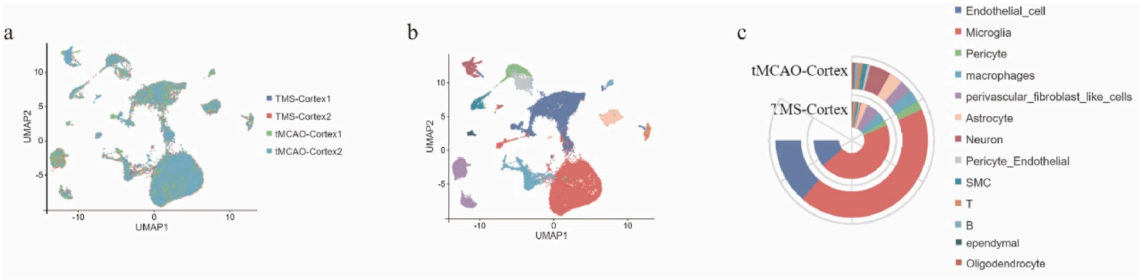

Fig. 2. Single-cell RNA sequencing of rat brains recapitulates the transcriptome profile of IS. **a.** UMAP plot displayed single-cell clusters colored according to their sample source. **b.** UMAP plot visualized single-cell clusters colored by cell type. **c.** The circular plot showed the relative expression changes of different cell types within each group.

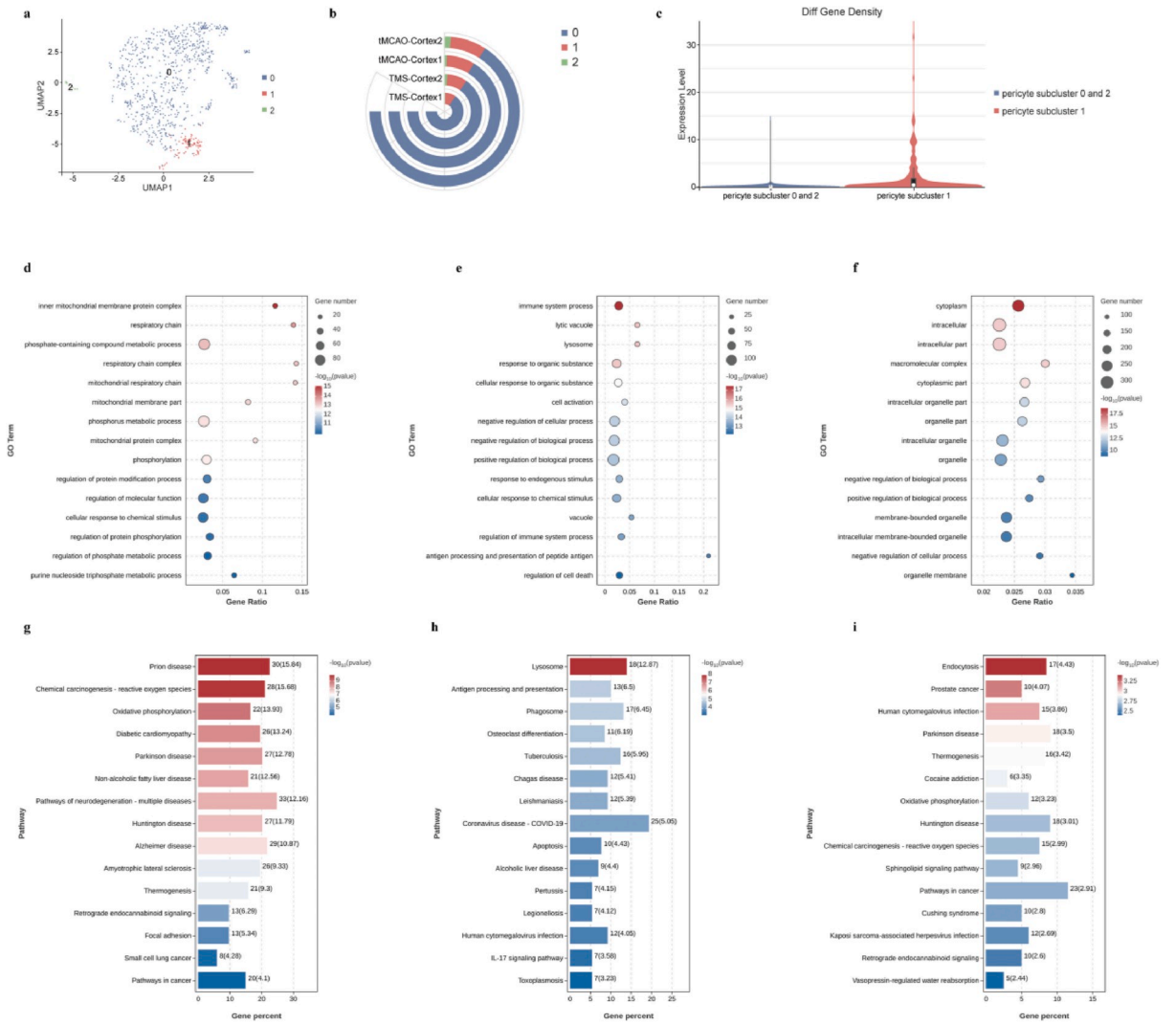

Fig. 3. Results of pericyte subclusters heterogeneity analysis. **a.** Visualization of UMAP plot for subcluster clustering of pericytes. **b.** Circular plot depicting relative expression changes of different pericyte subtypes. **c.** Violin plot showing the variation of upregulated genes Tnf, Il-1β, and Tgfbr1 among different subclusters. **d-f.** Bubble plots sequentially illustrate the top 15 enriched GO terms for pericyte subcluster 0, 1, and 2. **g-i.** Bar charts sequentially display the top 15 enriched pathways for pericyte subclusters 0, 1, and 2.

disease, chemical carcinogenesis - reactive oxygen species cluster, sphingolipid signaling pathway, cancer pathways, Cushing's syndrome, Kaposi's sarcoma-associated herpesvirus infection, retrograde endocannabinoid signaling, and vasopressin-regulated water reabsorption, among others (Fig. 2i). Moreover, we unexpectedly found significant upregulation of Tnf, Il-1β, and Tgfbr1 genes in pericyte subcluster 1 compared to the other two subclusters (Fig. 3c). Overall, we are inclined to define pericyte subcluster 1 as a more active cell type.

3.3. Intercellular communication network analysis of pericytes

We utilized the CellChat software package to investigate the ligand-receptor interactions among pericytes, endothelial cells, and SMC in different samples. The bubble plots of the intercellular subpopulation level ligand-receptor relationships indicated that the number and strength of ligand-receptor interactions were higher among pericyte-pericyte, endothelial cell-endothelial cell, and endothelial cell-pericyte subgroups after rTMS intervention (Fig. 4a, b, e).

The bubble plot depicting the signaling pathway communication between cell subclusters further revealed specific ligand-receptor relationships for each cell pair. Results showed that after rTMS intervention, new signaling pathways involving Lgals9-Havcr2, Lgals9-Cd45, Icam2-(Itgam + Itgb2), and Icam1-(Itgam + Itgb2) were formed between endothelial cells and pericytes. Additionally, pericytes established a signaling pathway with themselves through Icam1-(Itgam + Itgb2). The signaling pathway interactions between pericytes and vascular smooth muscle cells exhibited similarities to those observed in the relationship between endothelial cells and

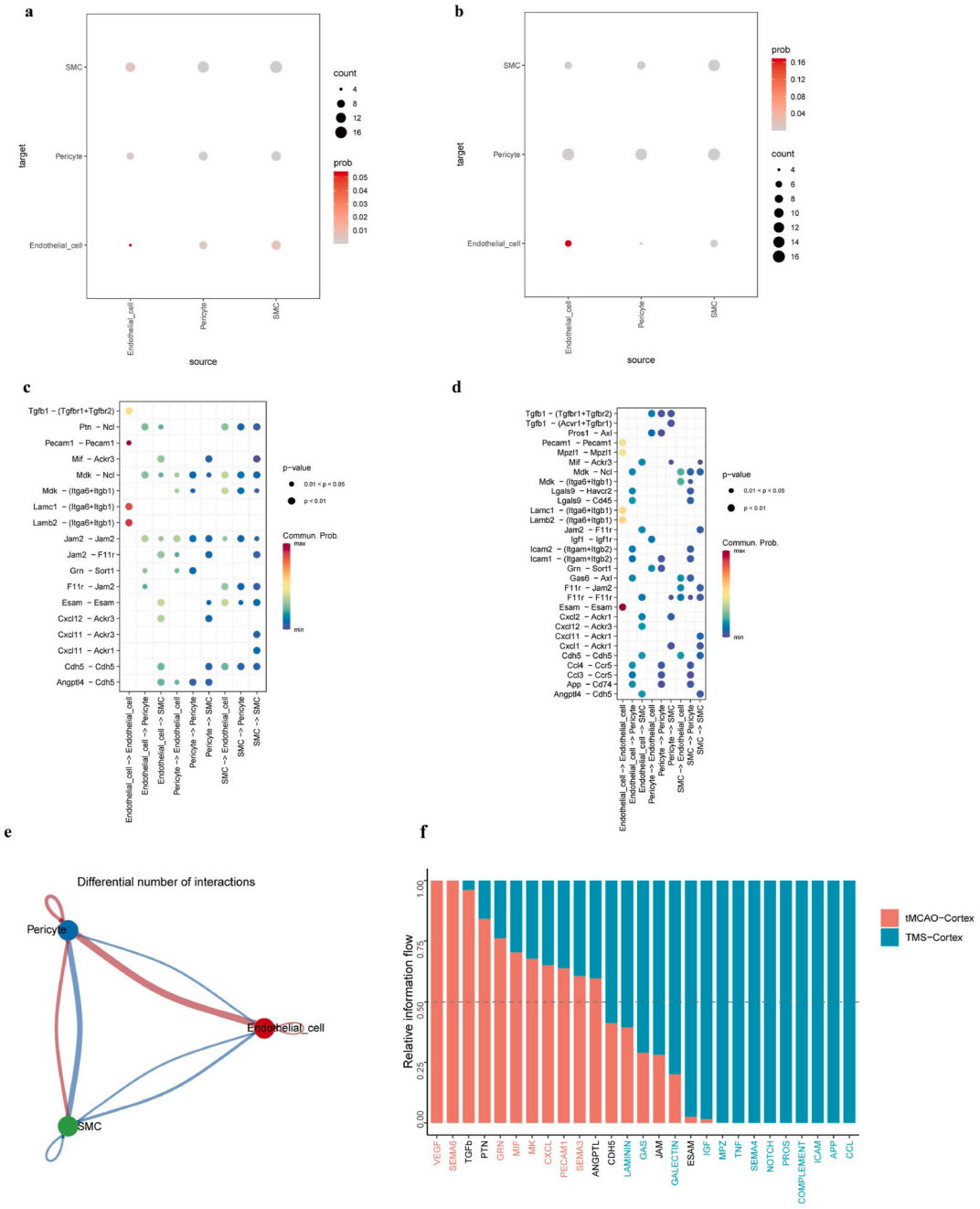

Fig. 4. Cell communication results in pericytes, endothelial cells, and SMC. **a.** The ligand-receptor relationships between cell subclusters in the tMCAO group were visually represented using a bubble plot. **b.** A bubble plot was used to illustrate the ligand-receptor relationships between cell subclusters in the rTMS group. **c.** The signaling pathway relationships between cell subgroups in the tMCAO group were depicted through a bubble plot. **d.** The signaling pathway relationships between cell subgroups in the rTMS group were demonstrated using a bubble plot. **e.** Changes in the ligand-receptor relationships between cell subclusters in the two groups were visualized using a network plot. The outer circles denoted pericytes, endothelial cells, and vascular smooth muscle cells, with the size of the circles indicating the quantity of ligand-receptor pairs present in each subcluster. Larger circles indicated a higher ratio of ligand-receptor pairs between cells. The blue lines represented cell communication in the tMCAO group, while the red lines represented cell communication in the rTMS group, with thicker lines indicating stronger communication intensity. **f.** Differential pathway enrichment between the tMCAO and rTMS groups was illustrated using a bar chart.

pericytes(Fig. 4c and d). Furthermore, a bar chart describing the differential enrichment of signaling pathways between groups showed enrichment of IGF, TNF, NOTCH, ICAM, and other signaling pathways after rTMS intervention (Fig. 4f).

3.4. Evolutionary analysis of pericytes, endothelial cells, and SMCs

We utilized the Monocle software package to perform pseudotime analysis of pericytes, SMCs, and endothelial cells, aiming to investigate their developmental differentiation. Pseudotime information revealed three distinct developmental stages and one branching point. (Fig. 5a). State 1 represented the initial developmental stage, followed by State 2 and State 3 (Fig. 5b). The DEGs at various stages throughout the developmental timeline were utilized for cellular annotation. This analysis hinted at a sequential developmental correlation among pericytes, SMCs, and endothelial cells, suggesting the potential of pericytes to differentiate into both SMCs and endothelial cells (Fig. 5c). Additionally, we found that VEGF-a, TGF-β, TNF, and other genes could act as fate-determining genes inducing differentiation towards State 2 and State 3 from State 1, thus promoting the developmental differentiation of pericytes (Fig. 5d, e,f).

3.5. Differentially expressed genes (DEGs) and functional annotation after rTMS intervention

To investigate changes in gene expression and functional annotations among pericytes, endothelial cells, and SMCs after rTMS intervention, we conducted GO and KEGG analyses on DEGs between the tMCAO group and rTMS group to elucidate the most representative processes and pathways. In contrast to the tMCAO group, the rTMS intervention mainly upregulated genes such as Bglap, S100a9, S100a8, Col1a1, and Hspb1, while downregulating genes such as Ttr, Rpl38, Enpp2, Gfap, and Rprml in pericytes (Fig. 6a). GO analysis focused primarily on biological processes, selecting the top 15 most enriched processes based on p-value. We observed significant enrichment of processes related to differentiation and development, regulation of biological processes, and stress response (Fig. 6d). KEGG analysis used p-value as a screening criterion and showed the top 15 enriched pathways, including protein processing in the endoplasmic reticulum, focal adhesion, human cytomegalovirus infection, ECM-receptor interaction, cancer pathways, human papillomavirus infection, cellular senescence, thyroid cancer, antigen processing and presentation, toxoplasmosis, prostate cancer, HIF-1 signaling pathway, chronic myeloid leukemia, complement and coagulation cascade, and endocytosis (Fig. 6g).

DEGs in endothelial cells exhibited similarities to those in pericytes. Specifically, genes such as S100a8, S100a9, Pf4, Fam111a, and Lyz2 were upregulated, while Ttr, Rpl38, Fabp7, Ccnd2, and Gfap were downregulated (Fig. 6b). GO analysis revealed enrichment of processes related to cell activation, single-organism developmental process, stress response, and regulation of biological processes (Fig. 6e). Additionally, KEGG analysis showed enrichment of multiple pathways, including phagosome, osteoclast differentiation, AGE-RAGE signaling pathway in diabetic complications, aldosterone-regulated sodium reabsorption, miRNAs in cancer, type I diabetes mellitus, shear stress and atherosclerosis, TNF signaling pathway, graft-versus-host disease, necroptosis, iron metabolism in humans, gap junction, legionellosis, MAPK signaling pathway, and human T-cell leukemia virus 1 infection (Fig. 6h).

Furthermore, we found that SMC mainly upregulated genes such as Bglap, S100a9, S100a8, Cym, and Reck, while downregulating Ttr, Rpl38, Enpp2, Sox4, and Cidea (Fig. 6c). Similarly, GO analysis primarily showed enrichment of processes such as blood vessel morphogenesis, localization regulation, intracellular signaling transduction, cellular component organization or biogenesis, stress

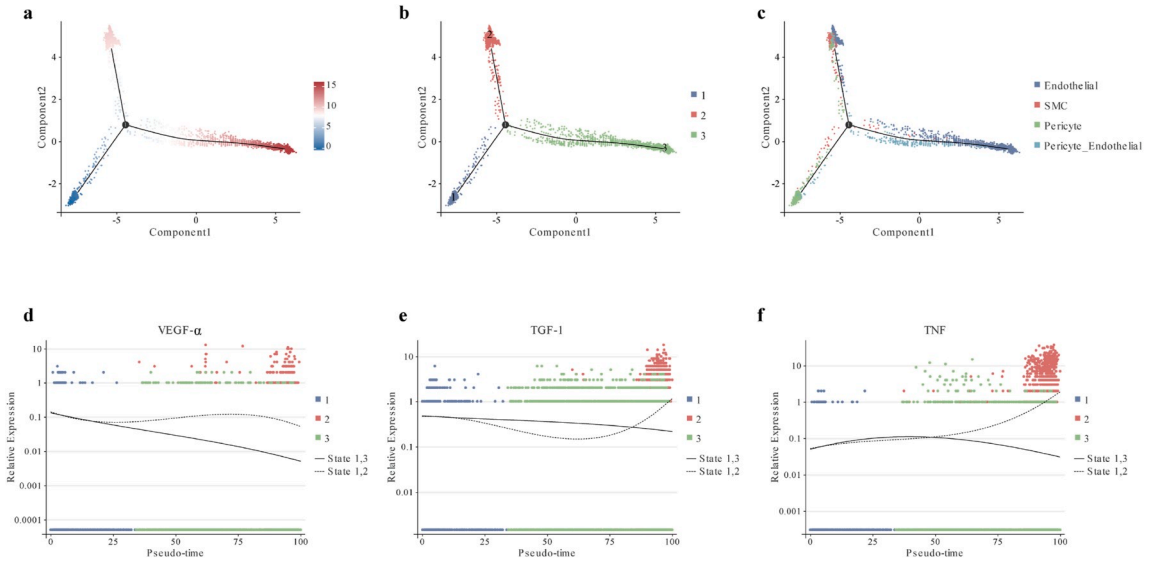

Fig. 5. Results of the proposed temporal analysis of pericytes. **a.** Developmental timeline of the pericyte subclusters. Lighter shades indicate lower Pseudotime values, representing early developmental stages. **b.** Pericyte subpopulations can be divided into 3 different developmental stages. **c.** Annotation of the 3 different developmental stages. **d-f.** Differential gene VEGF-a, TGF-β, and TNF expression in differentiation fate.

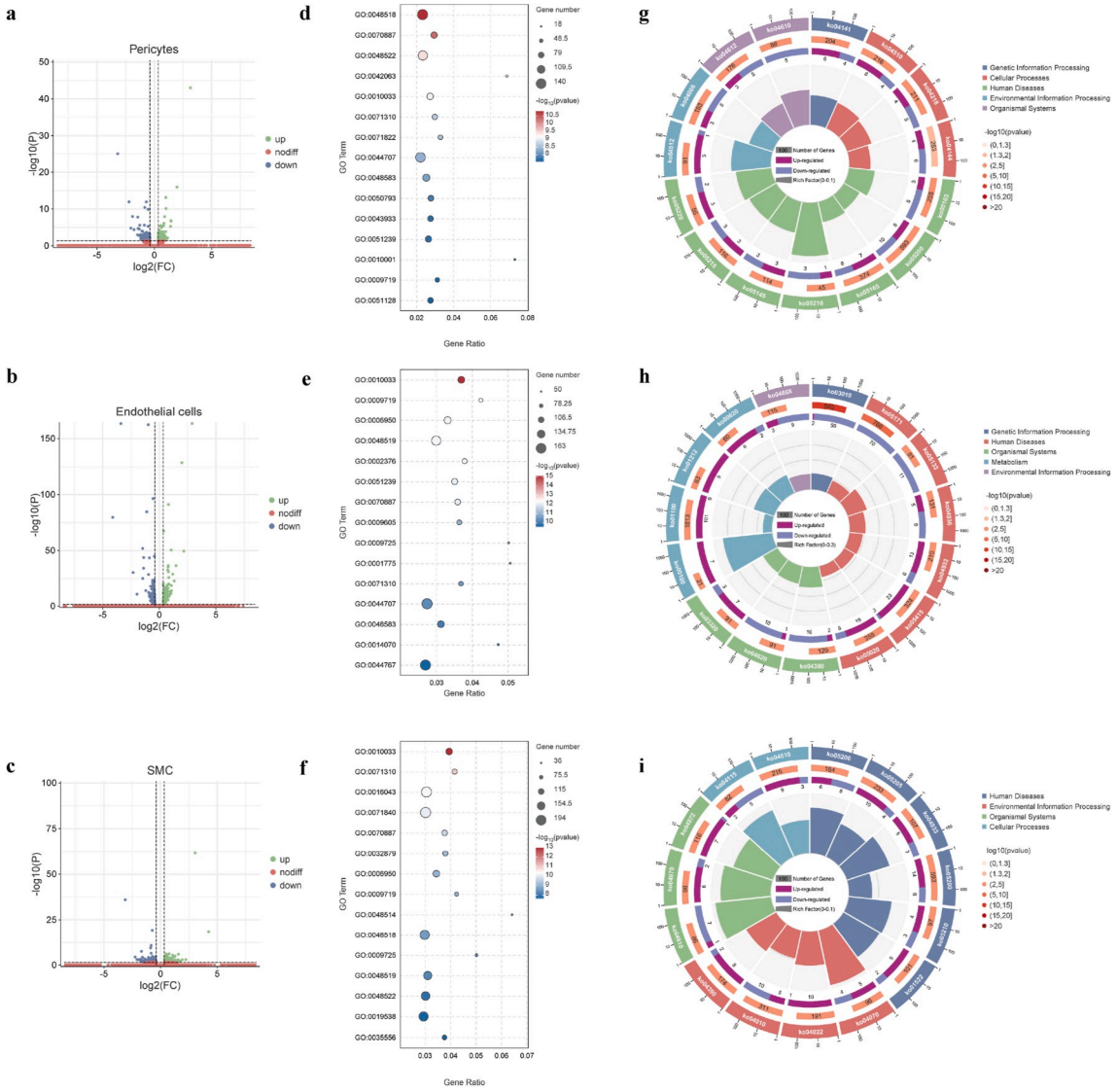

Fig. 6. DEGs and Functional Annotation following rTMS Intervention. **a-c.** The volcano plots sequentially demonstrated the DEGs in pericytes, endothelial cells, and SMCs, respectively. **d-f.** The bubble plots sequentially elucidated the top 15 enriched GO terms specific to pericytes, endothelial cells, and SMCs, respectively. **g-i.** The circular plots sequentially exhibited the top 15 enriched pathways unique to pericytes, endothelial cells, and SMCs, respectively.

response, and regulation of biological processes (Fig. 6f). KEGG analysis showed enrichment of pathways such as miRNAs in cancer, phosphatidylinositol signaling system, complement and coagulation cascades, proteoglycans in cancer, salivary secretion, p53 signaling pathway, AGE-RAGE signaling pathway in diabetic complications, focal adhesion, cGMP-PKG signaling pathway, MAPK signaling pathway, pancreatic secretion, hedgehog signaling pathway, cancer pathways, colorectal cancer, and insulin resistance (Fig. 6i).

4. Discussion

Stroke stands out as a primary factor contributing to adult disability, resulting in long-term functional impairments [1]. Stroke is characterized by disturbances in the BBB and increased permeability, which are associated with poor prognosis [18]. Therefore, the BBB can serve as a therapeutic target. Previous studies have demonstrated the relevance of BBB permeability to pericytes, SMCs, and endothelial cells [19,20]. As a promising method for addressing neurological impairments in individuals recovering from stroke, rTMS has shown effectiveness in alleviating motor dysfunction [21,22], dysphagia [12,23], aphasia [24,25], and post-stroke depression [26]. Two studies have demonstrated the efficacy of TMS in inducing the polarization of A2-type astrocytes and promoting angiogenesis, thereby exerting a neuroprotective effect in middle cerebral artery occlusion (MCAO) rats [27,28]. Furthermore, there exists

evidence suggesting the potential role of TMS in inducing the opening of the BBB [29]. However, the specific mechanisms underlying these effects remain ambiguous. While previous research has primarily centered on astrocytes and microglia in investigating the mechanisms of rTMS targeting stroke in animal models [30], our study has expanded this focus to include pericytes. In this study, we chose to use 20 Hz rTMS. The selection of this frequency was based on the preliminary research carried out by our experimental team, which verified the effectiveness of 20 Hz rTMS in enhancing neurological function in post-stroke rats. To investigate the dynamic changes and potential mechanisms of rTMS intervention on BBB in post-stroke conditions, we utilized single-cell sequencing analysis to examine the transcriptional characteristics of pericytes following 20 Hz rTMS treatment. This study is the inaugural exploration of the impacts of rTMS intervention on pericytes in the tMCAO model through single-cell sequencing analysis.

Our sequencing outcomes disclosed alterations in diverse types of brain cells, particularly the constituent cells of the BBB, subsequent to rTMS intervention after stroke. Due to the pivotal role of pericytes in maintaining the integrity of the BBB, we proceeded to delineate subpopulations of pericytes, identifying three distinct subclusters: pericyte subcluster 0, pericyte subcluster 1, and pericyte subcluster 2. This expanded the spectrum of cellular subtypes that were identified. Previous studies have initially categorized pericyte subtypes as type-1 and type-2 pericytes [31], A-type and B-type pericytes [32], or T-type and M-type pericytes [33]. In our study, we found that pericyte subcluster 1 can be classified as T-type pericytes. Moreover, we focused on the characteristics of pericyte subcluster 1 and found that compared with the other two subgroups, pericyte subcluster 1 displayed significant upregulation of genes such as TNF, IL-1β, and Tgfbr1. Functional annotation showed that it was involved in cell activation, stress response, immune regulation, and cell death regulation. These findings suggest that pericyte subcluster 1 may be a cellular group closely related to pericyte activation, differentiation, and development. The distinct transcriptome of this particular subcluster indicates promising targets for potential post-stroke treatments. Following rTMS intervention, a marginal rise in the proportion of pericyte subgroup 1 was noted; however, further investigation is essential to verify this finding.

Moreover, to further understand how pericytes influence BBB function, we analyzed their interactions with SMCs and endothelial cells. Supported by previous evidence, our findings highlight the potential of rTMS to enhance cellular communication among pericytes, endothelial cells, and SMCs, thereby fostering post-stroke vascular generation and regulating BBB permeability. Specifically, the Icam1-(Itgam + Itgb2) signaling pathway facilitates interactions between endothelial cells and pericytes, as well as among pericytes themselves. Furthermore, signaling pathways including IGF, TNF, NOTCH, and ICAM are found to be enriched in this process. Studies have demonstrated the significant involvement of IGF-1 in the development of neurovascular systems, nerve regeneration, and the growth of the central nervous system. Adhesion molecules and growth factors are closely linked to the activation, proliferation, and regeneration of endothelial cells. Moreover, under specific conditions, IGF-1 and TNF-a can synergistically upregulate ICAM-1 expression on endothelial cells, thereby activating them. Research has underscored the importance of the NOTCH signaling pathway in the maintenance, proliferation, and differentiation of neural stem cells (NSCs) [34], as well as in vascular formation and repair following brain injury [35]. Furthermore, the interaction between NOTCH1 signaling and VEGF-A has been confirmed, contributing to angiogenesis post-stroke [36].

Meantime, our results also revealed a temporal developmental relationship among pericytes, endothelial cells, and SMCs. Pericytes are at an early stage of development, while endothelial cells and SMCs develop later. Based on our findings, it is indicated that pericytes have the capacity to differentiate into both endothelial cells and SMCs, with VEGF-α, TGF-β, and TNF exhibiting distinct roles in promoting pericyte maturation. Pericytes and SMCs have historically been referred to as mural cells due to their close spatial association with endothelial cells in forming the vessel wall [37]. Our results enhance the understanding of the developmental dynamics among these cell types.

The SMC proliferation can be attributed to the maturation and differentiation of a portion of pericytes in our study, which aligns with previous findings [38]. However, there is ongoing debate regarding the differentiation relationship between pericytes and endothelial cells. Research shows that endothelial cells may be able to transform into cardiac pericytes and SMCs [39]. However, our study may contradict this idea. This discrepancy could be due to differences in tissue origins and the types of diseases being studied.

Nevertheless, the precise molecular pathways governing these interactions have yet to be completely understood. Hence, we proceeded with a more in-depth analysis of the DEGs following the rTMS intervention. DEGs in the pericytes were found to be enriched in stress, differentiation, and development-related biological processes. Analysis using the KEGG pathway database revealed that these DEGs were primarily associated with key pathways such as protein synthesis in the endoplasmic reticulum, the HIF-1 signaling pathway, focal adhesion, ECM-receptor interaction, and antigen processing and presentation. Similarly, DEGs in endothelial cells and pericytes displayed enrichment in cell activation and stress-related processes, with significant involvement in pathways related to miRNAs in cancer, the TNF signaling pathway, gap junctions, and the MAPK signaling pathway. Furthermore, SMCs showed enrichment in biological processes such as vascular morphogenesis, intracellular signaling transduction, localization regulation, and stress in intergroup analysis. KEGG analysis highlighted their association with miRNAs in cancer, the p53 signaling pathway, focal adhesion, and the MAPK signaling pathway.

In a study conducted by Zong et al. [13], the impact of θ-burst rTMS on a rat photothrombotic stroke model revealed that rTMS could trigger the activation of HIF-1α signaling. This led to the polarization of astrocytes related to vasculature into an A2 phenotype, thereby eliciting a protective and reparative influence on the peri-infarct microvascular system following a stroke. This finding further supports the beneficial role of rTMS in ischemic stroke. Moreover, in their study on intracerebral hemorrhage (ICH), Cui et al. [40] demonstrated that rTMS could boost the proliferation of neural stem cells and promote neuronal differentiation via the MAPK signaling pathway, thus alleviating neurofunctional impairments. These results collectively offer significant support for our research findings and indicate promising implications. Nonetheless, further comprehensive investigations are necessary to fully comprehend the underlying mechanisms.

At the same time, we observed Reck as one of the genes that were upregulated in the intergroup analysis of SMCs. Previous research

has shown that Reck acts as a negative regulator of MMPs, preventing cancer metastasis and improving prognosis by balancing MMP-2 and MMP-9 [41]. Reck plays a role in controlling vascular development by promoting the correct interaction between mural cells and endothelial tip cells, as well as by preserving the perivascular fibronectin matrix [42]. Serving as a specific receptor for Wnt7, Reck regulates the development of the central nervous system vasculature (CNS) and the formation of the BBB by activating the endothelial Wnt/β-catenin signaling pathway [43]. Ulrich et al. [44] emphasized that Reck is a crucial regulator of the canonical Wnt signaling pathway, which cascades with VEGF to promote brain vascular development. Drawing on the prior findings concerning the developmental interplay between pericytes and the outcomes acquired, we hypothesize that the activation of the canonical Wnt signaling pathway by rTMS could potentially stimulate the differentiation of pericytes into SMCs, leading to an increase in Reck expression. This mechanism may play a role in the formation of vascular bundles within the central nervous system (CNS) and the preservation of BBB integrity. Nevertheless, further investigation is necessary to confirm this conjecture.

4.1. Limitation

Our study focuses on employing bioinformatics to investigat alterations in BBB components post-stroke with high-frequency rTMS intervention. Nevertheless, it is constrained by a relatively small sample size and narrow sampling time points. Future improvements will entail further refinement via functional experiments.

In summary, our bioinformatics discoveries emphasize the potential advantageous impact of rTMS on cellular interactions and differentiation among pericytes, endothelial cells, and SMCs. Furthermore, it indicates the potential role of the classical Wnt signaling pathway in sustaining the stability of the BBB. Moreover, we have uncovered distinct transcriptomic profiles in pericytes that could represent promising targets for stroke therapy. The current understanding of the mechanisms underlying the post-stroke effects of rTMS is limited, and our findings not only may address this gap but also could present new insights and evidence for future clinical investigations and interventions.

Funding

This work was supported by the National Natural Science Foundation of China (grant number 82372569 to Hongmei Wen, grant number 82102668 to Chao Li, grant number 82002383 to Yilong Shan), Guangdong Basic and Applied Basic Research Foundation (grant number 2023A1515011138 to Hongmei Wen), Guangzhou Science and Technology Plan (grant number 2023A03J0214 to Hongmei Wen).

Availability of data and materials

The data that support the findings of this study are available from the corresponding authors upon reasonable request.

Ethics approval

All animal procedures in our study were approved by the Institutional Animal Ethical Committee of Sun Yat-Sen University and adhered strictly to the guidelines for the Care and Use of Laboratory Animals set forth by the National Institutes. Measures were taken to minimize any pain or discomfort experienced by the animals during the study.

Consent to participate

Not applicable.

Consent for publication

All the authors give the consent for the publication of identifiable details, which can include the text, figures and other materials in this manuscript.

CRediT authorship contribution statement

Jiantao Zhang: Writing – original draft, Methodology, Data curation, Conceptualization. **Jiena Hong:** Writing – review & editing, Methodology. **Jiemei Chen:** Software, Methodology, Conceptualization. **Fei Zhao:** Writing – review & editing. **Qiuping Ye:** Writing – review & editing. **Yilong Shan:** Writing – review & editing. **Chao Li:** Writing – review & editing, Supervision. **Hongmei Wen:** Writing – review & editing, Supervision.

Declaration of competing interest

All the authors declare no potential conflicts of interest.

Acknowledgements

We are extremely grateful for the assistance provided by the real-time interactive online data analysis platform Omicsmart (http://www.omicsmart.com) in our bioinformatics analysis process.

References

[1] W. Johnson, O. Onuma, M. Owolabi, et al., Stroke: a global response is needed, Bull. World Health Organ. 94 (9) (2016) 634–a.
[2] W. Wang, B. Jiang, H. Sun, et al., Prevalence, incidence, and mortality of stroke in China: results from a nationwide population-based survey of 480 687 adults, Circulation 135 (8) (2017) 759–771.
[3] P.T. Do, C.C. Wu, Y.H. Chiang, et al., Mesenchymal stem/stromal cell therapy in blood-brain barrier preservation following ischemia: molecular mechanisms and prospects, Int. J. Mol. Sci. 22 (18) (2021).
[4] E. Gonul, B. Duz, S. Kahraman, et al., Early pericyte response to brain hypoxia in cats: an ultrastructural study, Microvasc. Res. 64 (1) (2002) 116–119.
[5] Y. Hu, X.D. Hu, Z.Q. He, et al., Anesthesia/surgery activate MMP9 leading to blood-brain barrier disruption, triggering neuroinflammation and POD-like behavior in aged mice, Int. Immunopharm. 135 (2024) 112290.
[6] Y. Li, L. Zhou, H. Deng, et al., A switch in the pathway of TRPC3-mediated calcium influx into brain pericytes contributes to capillary spasms after subarachnoid hemorrhage, Neurotherapeutics : the journal of the American Society for Experimental NeuroTherapeutics (2024) e00380.
[7] E.A. Neuwelt, Mechanisms of disease: the blood-brain barrier, Neurosurgery 54 (1) (2004) 131–140, discussion 41-2.
[8] R. Paolinelli, M. Corada, F. Orsenigo, et al., The molecular basis of the blood brain barrier differentiation and maintenance. Is it still a mystery? Pharmacol. Res. 63 (3) (2011) 165–171.
[9] O. Oztop-Cakmak, I. Solaroglu, Y. Gursoy-Ozdemir, The role of pericytes in neurovascular unit: emphasis on stroke, Curr. Drug Targets 18 (12) (2017) 1386–1391.
[10] B.C. Campbell, P.J. Mitchell, T.J. Kleinig, et al., Endovascular therapy for ischemic stroke with perfusion-imaging selection, N. Engl. J. Med. 372 (11) (2015) 1009–1018.
[11] W. Hacke, M. Kaste, E. Bluhmki, et al., Thrombolysis with alteplase 3 to 4.5 hours after acute ischemic stroke, N. Engl. J. Med. 359 (13) (2008) 1317–1329.
[12] X. Liao, G. Xing, Z. Guo, et al., Repetitive transcranial magnetic stimulation as an alternative therapy for dysphagia after stroke: a systematic review and meta-analysis, Clin. Rehabil. 31 (3) (2017) 289–298.
[13] X. Zong, Y. Li, C. Liu, et al., Theta-burst transcranial magnetic stimulation promotes stroke recovery by vascular protection and neovascularization, Theranostics 10 (26) (2020) 12090–12110.
[14] J. Hong, J. Chen, C. Li, et al., High-frequency rTMS improves cognitive function by regulating synaptic plasticity in cerebral ischemic rats, Neurochem. Res. 46 (2) (2021) 276–286.
[15] X. Lin, P. Miao, J. Wang, et al., Surgery-related thrombosis critically affects the brain infarct volume in mice following transient middle cerebral artery occlusion, PLoS One 8 (9) (2013) e75561.
[16] M. Bieber, J. Gronewold, A.C. Scharf, et al., Validity and reliability of neurological scores in mice exposed to middle cerebral artery occlusion, Stroke 50 (10) (2019) 2875–2882.
[17] F. Guo, J. Lou, X. Han, et al., Repetitive transcranial magnetic stimulation ameliorates cognitive impairment by enhancing neurogenesis and suppressing apoptosis in the Hippocampus in rats with ischemic stroke, Front. Physiol. 8 (2017) 559.
[18] A. Shindo, T. Maki, E.T. Mandeville, et al., Astrocyte-derived pentraxin 3 supports blood-brain barrier integrity under acute phase of stroke, Stroke 47 (4) (2016) 1094–1100.
[19] M.A. MäE, L. He, S. Nordling, et al., Single-cell analysis of blood-brain barrier response to pericyte loss, Circ. Res. 128 (4) (2021) e46–e62.
[20] R.E. Haddock, T.H. Grayson, T.D. Brackenbury, et al., Endothelial coordination of cerebral vasomotion via myoendothelial gap junctions containing connexins 37 and 40, Am. J. Physiol. Heart Circ. Physiol. 291 (5) (2006) H2047–H2056.
[21] J. DU, L. Tian, W. Liu, et al., Effects of repetitive transcranial magnetic stimulation on motor recovery and motor cortex excitability in patients with stroke: a randomized controlled trial, Eur. J. Neurol. 23 (11) (2016) 1666–1672.
[22] J. Li, X.M. Meng, R.Y. Li, et al., Effects of different frequencies of repetitive transcranial magnetic stimulation on the recovery of upper limb motor dysfunction in patients with subacute cerebral infarction, Neural regeneration research 11 (10) (2016) 1584–1590.
[23] X. Wen, Z. Liu, L. Zhong, et al., The effectiveness of repetitive transcranial magnetic stimulation for post-stroke dysphagia: a systematic review and meta-analysis, Front. Hum. Neurosci. 16 (2022) 841781.
[24] A. Kielar, D. Patterson, Y.H. Chou, Efficacy of repetitive transcranial magnetic stimulation in treating stroke aphasia: systematic review and meta-analysis, Clin. Neurophysiol. : official journal of the International Federation of Clinical Neurophysiology 140 (2022) 196–227.
[25] J. Zhang, D. Zhong, X. Xiao, et al., Effects of repetitive transcranial magnetic stimulation (rTMS) on aphasia in stroke patients: a systematic review and meta-analysis, Clin. Rehabil. 35 (8) (2021) 1103–1116.
[26] W. Gao, F. Xue, B. Yu, et al., Repetitive transcranial magnetic stimulation for post-stroke depression: an overview of systematic reviews, Front. Neurol. 14 (2023) 930558.
[27] X. Zong, Y. Dong, Y. Li, et al., Beneficial effects of theta-burst transcranial magnetic stimulation on stroke injury via improving neuronal microenvironment and mitochondrial integrity, Translational stroke research 11 (3) (2020) 450–467.
[28] Y. Hong, Q. Liu, M. Peng, et al., High-frequency repetitive transcranial magnetic stimulation improves functional recovery by inhibiting neurotoxic polarization of astrocytes in ischemic rats, J. Neuroinflammation 17 (1) (2020) 150.
[29] A. Petrovskaya, A. Tverskoi, A. Medvedeva, et al., Is blood-brain barrier a probable mediator of non-invasive brain stimulation effects on Alzheimer's disease? Commun. Biol. 6 (1) (2023) 416.
[30] Y. Xing, Y. Zhang, C. Li, et al., Repetitive transcranial magnetic stimulation of the brain after ischemic stroke: mechanisms from animal models, Cell. Mol. Neurobiol. 43 (4) (2023) 1487–1497.
[31] A. Birbrair, T. Zhang, D.C. Files, et al., Type-1 pericytes accumulate after tissue injury and produce collagen in an organ-dependent manner, Stem Cell Res. Ther. 5 (6) (2014) 122.
[32] C. GöRITZ, D.O. Dias, N. Tomilin, et al., A pericyte origin of spinal cord scar tissue, Science (New York, NY) 333 (6039) (2011) 238–242.
[33] A.C. Yang, R.T. Vest, F. Kern, et al., A human brain vascular atlas reveals diverse mediators of Alzheimer's risk, Nature 603 (7903) (2022) 885–892.
[34] M.J. Xiao, Z. Han, B. Shao, et al., Notch signaling and neurogenesis in normal and stroke brain, International journal of physiology 1 (2) (2009) 192–202, pathophysiology and pharmacology.
[35] Q.S. Ran, Y.H. Yu, X.H. Fu, et al., Activation of the Notch signaling pathway promotes neurovascular repair after traumatic brain injury, Neural regeneration research 10 (8) (2015) 1258–1264.
[36] J. Zhu, Q. Liu, Y. Jiang, et al., Enhanced angiogenesis promoted by human umbilical mesenchymal stem cell transplantation in stroked mouse is Notch1 signaling associated, Neuroscience 290 (2015) 288–299.
[37] A. Lin, N.J. Peiris, H. Dhaliwal, et al., Mural cells: potential therapeutic targets to bridge cardiovascular disease and neurodegeneration, Cells 10 (3) (2021).
[38] A.T. Churchman, R.C. Siow, Isolation, culture and characterisation of vascular smooth muscle cells, Methods Mol. Biol. 467 (2009) 127–138.
[39] J.J. Patel, S. Srivastava, R.C. Siow, Isolation, culture, and characterization of vascular smooth muscle cells, Methods Mol. Biol. 1430 (2016) 91–105.
[40] M. Cui, H. Ge, H. Zeng, et al., Repetitive transcranial magnetic stimulation promotes neural stem cell proliferation and differentiation after intracerebral hemorrhage in mice, Cell Transplant. 28 (5) (2019) 568–584.

[41] J. Yuan, W. Li, J. Zhu, et al., Low expression of RECK in oral squamous cell carcinoma patients induces a shorter survival rate through an imbalance of RECK/MMPs, Int. J. Clin. Exp. Pathol. 13 (3) (2020) 501–508.
[42] G.M. DE Almeida, M. Yamamoto, Y. Morioka, et al., Critical roles for murine Reck in the regulation of vascular patterning and stabilization, Sci. Rep. 5 (2015) 17860.
[43] M. Vallon, K. Yuki, T.D. Nguyen, et al., A RECK-WNT7 receptor-ligand interaction enables isoform-specific regulation of Wnt bioavailability, Cell Rep. 25 (2) (2018), 339-49.e9.
[44] F. Ulrich, J. Carretero-Ortega, J. MenéNDEZ, et al., Reck enables cerebrovascular development by promoting canonical Wnt signaling, Development (Cambridge, England) 143 (6) (2016) 1055.